9

Dual Unscented Kalman Filter and Its Applications to Respiratory System Modelling

Esra Saatci[1] and Aydin Akan[2]
[1]*Istanbul Kultur University*
[2]*Istanbul University*
Turkey

1. Introduction

Unscented Kalman Filter (UKF) (Julier & Uhlmann, 1997) was developed as an improvement of Extended Kalman Filter (EKF) (Grewal & Andrews, 2001) for discrete-time filtering of the nonlinear dynamic systems. Comparison between different statistical approaches on the state and parameter estimation of the dynamic systems revealed that the performance of UKF is superior to EKF in many Kalman Filter (KF) applications (Chow et al., 2007); (Xiong et al., 2006); (Wan & Merwe, 2001); (Kandepu et al., 2008). Nonlinear dynamic systems with uncertain observations were often appeared in, for instance, communication systems (Wan & Merwe, 2001), medical systems (Polak & Mroczka, 2006) and machine learning (Chen, 2003). Medical systems, described by stochastic difference equations with measurement models including nonlinear and non-Gaussian components, are good candidates for the UKF analysis. Although there are many medical signal applications of Kalman Filters (KF); (Vauhkonen et al., 1998) and EKF (Avendano et al., 2006), some medical diagnostic and therapeutic measures are processed by UKF from indirect sensor measurements including statistical brain signal analysis to study cognitive brain functions by Electroencephalography (EEG) and functional Magnetic Resonance Imaging (fMRI) (Brochwell et al., 2007), ECG model-based denoising (Sameni et al., 2007), medical image processing (Ijaz et al., 2008), and evoke potential analysis in the neuroscience. These works demonstrated that UKF can be considered as an effective framework for medical signal analysing, modelling and filtering. Also, it was shown that UKF is a promising alternative in a variety of applications' domains including state and parameter estimation simultaneously which is dual estimation.

Respiratory mechanics is the dynamic relationship between appropriate pressures and flows in the respiratory system and assessment of it is an important problem in the diagnosis and monitoring of respiratory disorders, especially of Chronic Obstructive Pulmonary Disease (COPD). The primarily goal on the determination of the respiratory mechanics is the computation, or estimation, of the respiratory parameters non-invasively, continuously, effectively and without any patient cooperation. Direct approach to this problem is the measurement of the mechanics by the lung catheter or the alveolar capsule (Bates & Lutchen, 2005). However, these direct measurement methods are invasive and not suitable for continuous monitoring. On the other hand, the studies revealed that analysis of pressure

Source: Kalman Filter: Recent Advances and Applications, Book edited by: Victor M. Moreno and Alberto Pigazo,
ISBN 978-953-307-000-1, pp. 584, April 2009, I-Tech, Vienna, Austria

and flow signals measured at the airway opening represent the respiratory parameters in question while isolation of the peripheral information on the mechanics remains challenging (Bates & Lutchen, 2005). To achieve the goal of extracting the mechanical information from the measured pressure and flow signals at the mouth, investigators are now using advanced system identification techniques in frequency-domain, time-domain or time-frequency domain (Yuan et al., 1998); (Lutchen & Costa, 1990).

In the literature, common approach to respiratory mechanics determination is the inverse modelling of the respiratory system in the frequency-domain by measured overall impedance over the range of frequencies (Hellinckx et al., 2001). Although, the parameters of the inverse model is assumed to correspond to the physiologically important quantities, due to the simplifications on the model, interpretation of the parameters are not straightforward. Thus, determining the physiologically relevant information requires realistic multi-parameter models incorporating dynamic and nonlinear nature of the respiratory system. Measured data fitting to such a nonlinear model is very difficult in frequency-domain (Nucci et al., 2002). Moreover, most patients with COPD require artificial ventilatory supports that apply a positive pressure to the airway opening of the patient to assist ventilatory muscles and patient-ventilator interaction is a time-varying system (Nucci et al., 2002).

These shortcomings of frequency-domain analysis of the respiratory system led us to implement time-domain methods for the determination of the respiratory mechanics. Recently presented nonlinear dynamic RC model of the respiratory system (Saatci & Akan, 2007) and multi-parameter well-known Mead model (Diong et al., 2007) were selected for the inverse modelling of the respiratory system in the time-domain. Dual UKF method was applied to the respiratory models to estimate the states as well as the parameters. Time series were measured from both the COPD patients and healthy subjects and artificially produced by the model equations. The reason to use dual estimation was the complications of the model's state and measurement equations and nonlinear relationship between the parameters and the states of the respiratory models. In this respect, first, in the Section 3 EKF, UKF principles will be given briefly, and dual UKF algorithm will be discussed in details. Used respiratory models will be presented in the Section 4 and Section 5 is devoted to the estimation of the states and parameters of the models. Finally, results are given in Section 6 and in Section 7 conclusions are drawn.

2. Kalman filtering

EKF and UKF are the Bayesian data analysis based practical methods for the nonlinear system modelling from the observed data using probability models for both the unobserved states and the unknown system parameters. Many of the practical systems can be represented by the following state-space model:

$$\mathbf{x}_k = f_k\left(\mathbf{x}_{k-1}, \boldsymbol{\theta}, \mathbf{u}_k\right) + \mathbf{q}_k \tag{1}$$

$$\mathbf{z}_k = h_k\left(\mathbf{x}_k, \boldsymbol{\theta}, \mathbf{u}_k\right) + \mathbf{r}_k \tag{2}$$

where $f(\bullet)$ and $h(\bullet)$ are the generally nonlinear functions. $\mathbf{q}_k$ and $\mathbf{r}_k$ the are additive state and observation noises respectively. $\mathbf{u}_k$ is devoted to the known inputs and $\boldsymbol{\theta}$ is the unknown parameter vector of interest.

In the statistical analysis terms above equations are called state-observation models of the practical system and represented as the distributions $\mathbf{Pr}(\mathbf{x}_k/\mathbf{x}_{k-1},\boldsymbol{\theta})$ for the state vector $\mathbf{x}_k$ and $\mathbf{Pr}(\mathbf{z}_k/\mathbf{x}_k,\boldsymbol{\theta})$ for the observation equation. From the Bayesian perspective, the solution of (1) and (2) is to recursively estimate the state vector $\mathbf{x}_k$ and/or parameter vector $\boldsymbol{\theta}$ given the observations $\mathbf{Z}_k = \{\mathbf{z}_i\}_{i=1}^k$. Once the initial distributions $\mathbf{Pr}(\mathbf{x}_0,\boldsymbol{\theta})$ and $\mathbf{Pr}(\mathbf{x}_0/\mathbf{z}_0)$ are given, filtering posterior distribution $\mathbf{Pr}(\mathbf{x}_k/\mathbf{Z}_k,\boldsymbol{\theta})$ can be obtained recursively by two steps: prediction and filtering. In the prediction step with the help of Markov property of the state vector $\mathbf{x}_k$ predictive distribution $\mathbf{Pr}(\mathbf{x}_k/\mathbf{Z}_{k-1})$ is compute by:

$$\mathbf{Pr}(\mathbf{x}_k/\mathbf{Z}_{k-1},\boldsymbol{\theta}) = \int \mathbf{Pr}(\mathbf{x}_k/\mathbf{x}_{k-1},\boldsymbol{\theta})\mathbf{Pr}(\mathbf{x}_{k-1}/\mathbf{Z}_{k-1},\boldsymbol{\theta})d\mathbf{x}_{k-1} \tag{3}$$

In the filtering step posterior distribution is obtained based on the predictive distribution via Bayes' rule:

$$\begin{aligned}\mathbf{Pr}(\mathbf{x}_k/\mathbf{Z}_k,\boldsymbol{\theta}) &= \mathbf{Pr}(\mathbf{z}_k/\mathbf{x}_k,\boldsymbol{\theta})\mathbf{Pr}(\mathbf{x}_k/\mathbf{Z}_{k-1},\boldsymbol{\theta})/\mathbf{Pr}(z_k/Z_{k-1}) \\ &\propto \mathbf{Pr}(\mathbf{z}_k/\mathbf{x}_k,\boldsymbol{\theta})\mathbf{Pr}(\mathbf{x}_k/\mathbf{Z}_{k-1},\boldsymbol{\theta})\end{aligned} \tag{4}$$

Equations (3) and (4) constitute the recursive Bayesian estimation and are optimum in the sense that it seeks the posterior distribution which integrated and uses all of available information expressed by probabilities. However, direct computation of these disributions is not easy due to large state-observation space and multidimensional integrals. Thus above expression is considered as the theoretic foundation for the estimation problem and computations of the predictive and posterior distributions require certain limitations to the model.

2.1 Extended Kalman filter

If the model equations (1) and (2) were to be in the linear form and the process and observation noises were assumed to be zero-mean white Gaussian noises, $\mathbf{q}_k \sim N[0,Q]$ and $\mathbf{r}_k \sim N[0,R]$, celebrated Kalman Filter would be the Minimum Variance Unbiased Estimation (MVUE) providing an exact solution for the linear system with relatively easy matrix calculations. However, if the linearity and Gaussian distribution assumptions were violated, different approaches would be required to overcome the filtering problem (Arulampalam et al., 2002).

One of the methods developed for the solution of the nonlinear but Gaussian distributed systems is the EKF. In the EKF, nonlinearity is overcome by locally linearization of the model equations. Due to the Gaussian assumption of the posterior distribution, EKF works well for some types of nonlinear problems, but it may provide a poor performance in some cases when the true posterior is non-Gaussian. Thus, with the linearization and Gaussian assumption of the distributions, the EKF equations derived from the Kalman Filter theory are:

Prediction step:

$$\begin{aligned}\mathbf{x}_{k/k-1} &= f_k\left(\mathbf{x}_{k-1/k-1},\boldsymbol{\theta},\mathbf{u}_{k-1}\right) \\ \mathbf{P}_{k/k-1} &= \mathbf{F}_k\mathbf{P}_{k-1/k-1}\mathbf{F}_k^T + \mathbf{Q}\end{aligned} \tag{5}$$

$$K_k = \mathbf{P}_{k/k-1}\mathbf{H}_k^T\left(\mathbf{H}_k\mathbf{P}_{k/k-1}\mathbf{H}_k^T + \mathbf{R}\right)^{-1}$$

Filtering step:
$$\mathbf{x}_{k/k} = \mathbf{x}_{k/k-1} + K_k\left(\mathbf{z}_k - h_k\left(\mathbf{x}_{k/k-1}, \boldsymbol{\theta}, \mathbf{u}_k\right)\right) \quad (6)$$

$$\mathbf{P}_{k/k} = \left(I - K_k\mathbf{H}_k\right)\mathbf{P}_{k/k-1}$$

where $\mathbf{F}_k$ and $\mathbf{H}_k$ matrices are defined as:

$$\mathbf{F}_k = \left.\frac{df_k\left(\mathbf{x}, \boldsymbol{\theta}, \mathbf{u}_{k-1}\right)}{d\mathbf{x}}\right|_{\mathbf{x}=\mathbf{x}_{k-1/k-1}} \quad (7)$$

$$\mathbf{H}_k = \left.\frac{dh_k\left(\mathbf{x}, \boldsymbol{\theta}, \mathbf{u}_k\right)}{d\mathbf{x}}\right|_{\mathbf{x}=\mathbf{x}_{k/k-1}} \quad (8)$$

2.2 Unscented Kalman filter

Different from EKF, UKF is global method which attempts to solve whole posterior distribution by deterministic sampling approximation. Unscented Transformation (UT) where so-called sigma points are the deterministic samples from posterior distribution and propagate the information of the data through nonlinear transformation is the theory behind UKF. Thus, based on Kalman Theory, implementation of UKF can be summarized as follows:

Step 1: Initialization and weights calculations:

Draw N_x - dimensional particles $\mathbf{x}_0 = \left\{x_0^{(i)}\right\}_{i=1}^{N_x}$ from the prior distribution $\mathbf{Pr}\left(\mathbf{x}_0, \boldsymbol{\theta}\right) = \mathrm{N}\left(\mathbf{x}_0, \mathbf{P}_0\right)$.

$$w_m^{(i)} = \lambda/\left(N_x + \lambda\right) \qquad i = 0$$
$$w_c^{(i)} = \lambda/\left(N_x + \lambda\right) + \left(1 - \alpha^2 + \beta\right) \qquad i = 0$$
$$w_m^{(i)} = w_c^{(i)} = 1/2\left(N_x + \lambda\right) \qquad i = 1, \ldots 2N_x$$

where $\lambda = \alpha^2\left(N_x + \kappa\right) - N_x$ is the composite scaling parameter and determines the spread of the sigma points around $\mathbf{x}_k$. α, β and κ are the parameters for scaling and prior distribution of $\mathbf{x}_0$.

For $k = 1, \ldots \infty$

Step 2: Sigma points calculations 1:

$$\aleph_{k-1}^{(i)} = \mathbf{x}_{k-1} \qquad i = 0$$
$$\aleph_{k-1}^{(i)} = \mathbf{x}_{k-1} + \left(\sqrt{\left(N_x + \lambda\right)\mathbf{P}_{k-1}}\right)_{(i)} \qquad i = 1, \ldots N_x$$
$$\aleph_{k-1}^{(i)} = \mathbf{x}_{k-1} - \left(\sqrt{\left(N_x + \lambda\right)\mathbf{P}_{k-1}}\right)_{(i)} \qquad i = N_x + 1, \ldots 2N_x$$

where $\left(\sqrt{\left(N_x + \lambda\right)\mathbf{P}_{k-1}}\right)_{(i)}$ is the i th column of the matrix.

Step 3: Prediction:

$$\aleph_{k/k-1}^{(i)} = f_k\left(\aleph_{k-1}^{(i)}, \boldsymbol{\theta}, \mathbf{u}_{k-1}\right) \quad i = 0, \ldots 2N_x$$

$$\mathbf{x}_{k/k-1} = \sum_{i=0}^{2N_x} w_m^{(i)} \aleph_{k/k-1}^{(i)}$$

$$\mathbf{P}_{k/k-1} = \sum_{i=0}^{2N_x} w_c^{(i)} \left(\aleph_{k/k-1}^{(i)} - \mathbf{x}_{k/k-1} \right) \left(\aleph_{k/k-1}^{(i)} - \mathbf{x}_{k/k-1} \right)^T + \mathbf{Q}$$

Step 4: Sigma points calculations 2:

$$\aleph_{k/k-1}^{(i)*} = \mathbf{x}_{k/k-1} \qquad i = 0$$

$$\aleph_{k/k-1}^{(i)*} = \mathbf{x}_{k/k-1} + \left(\sqrt{(N_x + \lambda)\mathbf{P}_{k/k-1}} \right)_{(i)} \qquad i = 1, \ldots N_x$$

$$\aleph_{k/k-1}^{(i)*} = \mathbf{x}_{k/k-1} - \left(\sqrt{(N_x + \lambda)\mathbf{P}_{k/k-1}} \right)_{(i)} \qquad i = N_x + 1, \ldots 2N_x$$

Step 5: Filtering:

$$Z_{k/k-1}^{(i)} = h_k \left(\aleph_{k/k-1}^{(i)*}, \boldsymbol{\theta}, \mathbf{u}_{k-1} \right)$$

$$\mathbf{z}_{k/k-1} = \sum_{i=0}^{2N_x} w_m^{(i)} Z_{k/k-1}^{(i)}$$

$$\mathbf{P}_{zz} = \sum_{i=0}^{2N_x} w_c^{(i)} \left(Z_{k/k-1}^{(i)} - \mathbf{z}_{k/k-1} \right) \left(Z_{k/k-1}^{(i)} - \mathbf{z}_{k/k-1} \right)^T + \mathbf{R}$$

$$\mathbf{P}_{xz} = \sum_{i=0}^{2N_x} w_c^{(i)} \left(\aleph_{k/k-1}^{(i)*} - \mathbf{x}_{k/k-1} \right) \left(Z_{k/k-1}^{(i)} - \mathbf{z}_{k/k-1} \right)^T$$

$$K_k = \mathbf{P}_{xz} \mathbf{P}_{zz}^{-1}$$

$$\mathbf{x}_k = \mathbf{x}_{k/k-1} + K_k \left(\mathbf{z}_k - \mathbf{z}_{k/k-1} \right)$$

$$\mathbf{P}_k = \mathbf{P}_{k/k-1} - K_k \mathbf{P}_{zz} K_k^T$$

Above algorithm is based on the conventional UKF, however there are variant UKF algorithms proposed in the literature. For instance, Unscented Particle Filter (UPF) is the most important one among them. In UPF, UKF is used to optimize the sampling stage of the Particle Filter (PF) by generating the required samples from $\mathbf{Pr}(\mathbf{x}_k / \mathbf{Z}_k, \boldsymbol{\theta})$ rather than $\mathbf{Pr}(\mathbf{x}_k / \mathbf{x}_{k-1}, \boldsymbol{\theta})$. As PF makes no assumption on the form of the probability densities in question, UPF is most suited to non-Gaussian systems. Another variant of UKF is the square-root implementation of the UKF algorithm where *Cholesky factor* is used for the matrix square-root of the state/parameter covariance matrix. Then the *Cholesky factor* is propagated via *QR decomposition* in subsequent iterations. This form of the UKF algorithm is mostly required where the convergence speed or execution duration is important.

2.3 Dual unscented Kalman filter

System identification often requires simultaneous state and parameter estimation from observed noisy data. If the parameters are assumed to have a prior distribution, $\mathbf{Pr}(\boldsymbol{\theta})$ Bayesian approach can be also applied to the parameter estimation. Therefore UKF equations above are modified for the dual estimation problem in order to extend the advantages of UKF method to the parameter estimation. There are two common

approaches for the simultaneous estimation: estimation with two different state-observation models or estimation by augmented state model with common observation model. First called dual UKF incorporates two distinct sequential filters, one estimating the true states and the other estimating the parameters. Later is called joint UKF and implementation not much differs from the UKF algorithm.
If the parameters of the dynamic system are considered as time-invariant random variables that need to be estimated, time-update should allow no changes beyond the effects of state noise. That is modelled as a first-order Markov process:

$$\boldsymbol{\theta}_{k+1} = \boldsymbol{\theta}_k + \mathbf{q}_p^k \tag{9}$$

where $\mathbf{q}_p^k \sim N\left[0, Q_p\right]$ is the parameter process noise and assumed to be zero-mean white Gaussian noise.
However, expression in (9) may not suitable for the systems where the parameters are actually constant unknowns. Thus, for those systems the parameter state noise is not existed at all and should not be added to the model. The parameter time-update becomes:

$$\boldsymbol{\theta}_{k+1} = \boldsymbol{\theta}_k \tag{10}$$

This form of the state equation of the parameters considerably simplifies the UKF algorithm. Thus, in the dual UKF algorithm, at the parameter estimation stage step 2 and step 3 are replaced by the equation (5) where $f(\bullet)$ and $\mathbf{F}_k$ are the identity matrices.
Constraints due to the physical limitations on the parameters are also applied to the dual estimation problem. Parameter constraints are usually represented by the box constraints ($\boldsymbol{\theta}_{\mathbf{L}} \le \boldsymbol{\theta} \le \boldsymbol{\theta}_{\mathbf{H}}$). In the respiratory models, parameters are assumed to be positive real numbers, thus the constraints are defined as $0 \le \boldsymbol{\theta} \le \infty$. Modifications to the dual algorithm should be made due to the constraints in the models. In the algorithm, after the sigma pints were calculated (Step 2) and the Prediction step (Step 3), constrained sigma points were obtained with the projection method explained in (Moradkhani et al., 2005). The new constrained sigma points are defined as $\aleph_{k-1}^{(i),C} = P\left(\aleph_{k-1}^{(i)}\right)$ and $\aleph_{k/k-1}^{(i),C} = P\left(\aleph_{k/k-1}^{(i)}\right)$.

3. Respiratory models

Respiratory models express the viscoelastic and mechanic properties of the airways, lung and chestwall and these properties are usually represented by the electrical elements. Elemental equations define the relationship between appropriate pressures and volumetric flow at the specific regions of respiratory system whereas the system state and measurement equations are the mathematical descriptions of the whole system behaviour. Theoretical and experimental studies reveal that respiratory system models may be linear and nonlinear in both state and parameters depending on the system identification technique, considered disease conditions and experimental methodology (Polak & Mroczka, 2006); (Bates & Lutchen, 2005); (Avanzolini et al., 1995). For the interested reader, discussion and comparisons on the linear and nonlinear models can be found in the literature (Diong et al., 2007); (Yuan et al., 1998). In this work well-known multi-parameter linear Mead model and recently presented nonlinear RC model were used to model the respiratory system. The presented nonlinear model is the simplified model by (Athanasiades et al., 2000). The

motivation behind to use this nonlinear model was that, first it includes nonlinearities as well as time-varying nature of the respiratory system, second model states and measurements mimic the COPD patients data under non-invasive ventilatory support.

3.1 Mead respiratory model

Mead respiratory model with non-invasive ventilatory pressure effect, $P_{ven}(t)$ and muscular pressure effect, $P_{mus}(t)$ is shown in Fig. 1a. In the model, R_c and R_p are the resistances of the central and peripheral airways respectively. Airway flow inertance is represented as L and compliances include bronchial tube compliance C_b, lung compliance C_l, and chestwall compliance C_w.

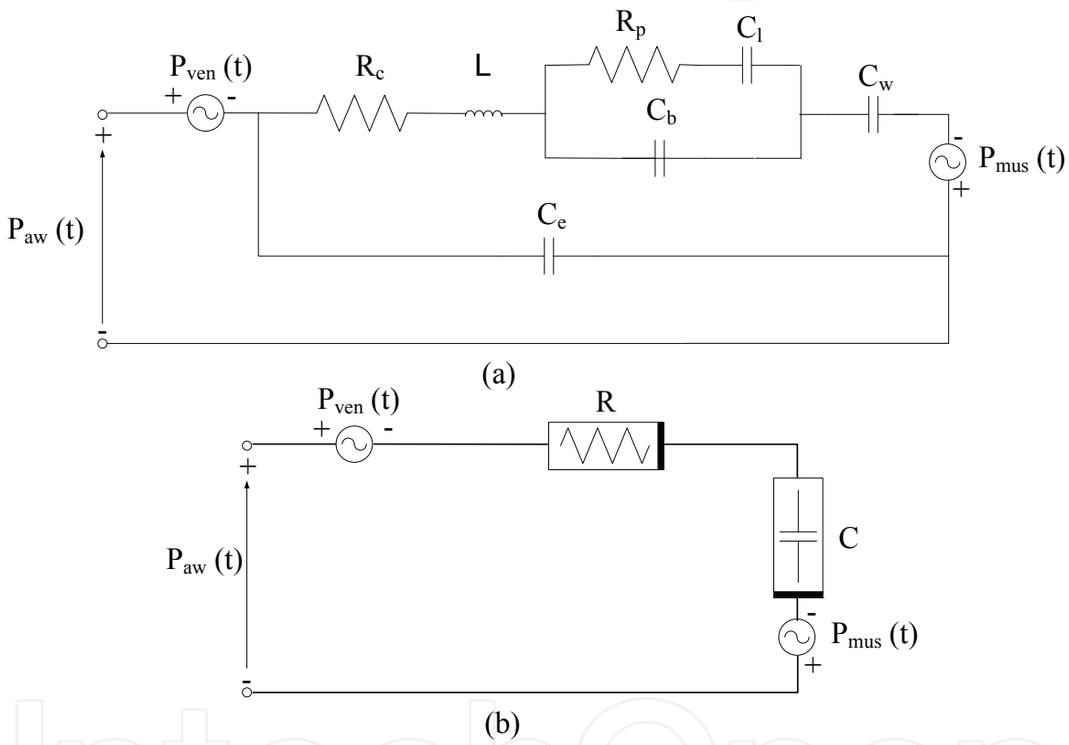

Fig. 1. (a) Mead respiratory model and (b) Nonlinear RC model of the respiratory system. Non-invasive ventilatory pressure effect, $P_{ven}(t)$ and muscular pressure effect, $P_{mus}(t)$ is added to the models.

Since the pressure measured at the airway opening is composed of relatively small part of the patient's effort and big part of the non-invasive ventilatory support, a series of the independent pressure sources are added to the model to mimic the muscular pressure effect and ventilatory effects. $P_{mus}(t)$ is direct effects of the patients inspiratory muscles and can be approximated by the second-order polynominal function (Yamada & Du, 2000):

$$P_{mus}(t) = \begin{cases} -P_{mus\,\mathbf{max}}\left(1 - t/T_I\right)^2 + P_{mus\,\mathbf{max}} & 0 \le t \le T_I \\ P_{mus\,\mathbf{max}} e^{-t/\tau_m} & T_I \le t \le T \end{cases} \tag{11}$$

where $P_{mus\,\mathbf{max}}$ represents the effect of maximal patient's effort and added to the unknown parameter vector. T_I and T are the inspiration duration time and total duration of one cycle respiration respectively. They are set to constant values in the algorithm. τ_m is the inspiratory muscles relaxation time constant and determines the patient-ventilator asynchrony. τ_m is also set to $60\,ms$ constant value in the simulations.
Non-invasive ventilator pressure is simulated as an exponential function (Yamada & Du, 2000):

$$P_{ven}(t)=\begin{cases} PEEP & 0\le t\le t_{trig} \\ P_{ps}\left(1-e^{-t/\tau_{vi}}\right) & t_{trig}\le t\le T_I \\ P_{ps}e^{-t/\tau_{ve}} & T_I\le t\le T \end{cases} \tag{12}$$

where P_{ps} represents the maximum inspiration pressure set on the non-invasive ventilator. Depended upon the patient's established values, P_{ps} is taken between $8\,cmH_20$ - $15\,cmH_20$ and Positive End Expiration Pressure (PEEP) is set to $0\,cmH_20$ - $4\,cmH_20$. Ventilator inspiration time constant τ_{vi} corresponds the flow acceleration speed of the ventilator, whereas ventilator expiration time constant τ_{ve} is the ventilator deceleration speed and contributes to the small pressure rise at the termination of the inspiration. Both τ_{vi} and τ_{ve} were set to $0.006\,s$. The inspiration trigger delay of the ventilator t_{trig} was set to $20\,ms$ corresponding to the real world scenario.
Above set values for $P_{mus}(t)$ and $P_{ven}(t)$ were applied to simulations where artificially produced data and COPD patient's data were used. For the healthy subject's data $P_{ven}(t)$ was not included to the respiration model.
In the Mead model, parameter vector and state vector can be defined respectively as: $\boldsymbol{\theta}_k=\left[R_c \quad L \quad C_l \quad C_b \quad R_p \quad C_w \quad C_e \quad P_{mus\,\mathbf{max}}\right]^T$, $\mathbf{x}_s^k=\left[\dot{V}_L^k \quad P_{C_l}^k \quad P_{C_b}^k \quad P_{C_w}^k \quad P_{C_e}^k\right]^T$. Then, with the help of basic electrical circuits rules and first-order Taylor series expansion the state-observation equations of the state vector in the discrete-time become:

$$\mathbf{x}_s^{k+1}=\begin{bmatrix} 1-R_c/L & 0 & -1/L & -1/L & 1/L \\ 0 & 1-1/R_pC_l & 1/R_pC_l & 0 & 0 \\ 1/C_b & 1/R_pC_b & 1-1/R_pC_b & 0 & 0 \\ 1/C_w & 0 & 0 & 1 & 0 \\ -1/C_e & 0 & 0 & 0 & 1 \end{bmatrix}\mathbf{x}_s^k+\begin{bmatrix} 0 \\ 0 \\ 0 \\ 0 \\ 1/C_e \end{bmatrix}\dot{V}_k+\begin{bmatrix} 1 \\ 0 \\ 0 \\ 0 \\ 0 \end{bmatrix}P_{mus}^k+\mathbf{q}_{ms}^k \tag{13}$$

$$\mathbf{z}_s^k=\begin{bmatrix}0 & 0 & 0 & 0 & 1\end{bmatrix}\mathbf{x}_s^k+P_{ven}^k+\mathbf{r}_{ms}^k \tag{14}$$

where k is the discrete-time index and we assumed that initial state vector $\mathbf{x}_s^0$ is 5-dimentional random vector with mean $E\left[\mathbf{x}_s^0\right]=\bar{\mathbf{x}}_s$ and covariance $E\left[\left(\mathbf{x}_s^0-\bar{\mathbf{x}}_s\right)\left(\mathbf{x}_s^0-\bar{\mathbf{x}}_s\right)^T\right]=P_s^0$, measurement noise and state noise are zero-mean white Gaussian noises, $\mathbf{q}_{ms}^k\sim N\left[0,Q_{ms}\right]$ and $\mathbf{r}_{ms}^k\sim N\left[0,R_{ms}\right]$. $\dot{V}_k$ is the measured airway flow sequence.

In order to define state-observation equations of the parameter vector, we assume that the parameters are first-order Markov process, but there is no uncertainty in the state $\mathbf{q}_{vp}^{k} \cong 0$. This means parameters are actually time-invariant. Thus the state-observation equations of the parameters are in the form as:

$$\boldsymbol{\theta}_{k+1} = \boldsymbol{\theta}_k \tag{15}$$

$$\mathbf{x}_s^{k+1} = h_k\left(\mathbf{x}_s^k, \boldsymbol{\theta}_k, \dot{V}_k, P_{mus}^k\right) + \mathbf{r}_{mp}^k \tag{16}$$

where we assumed that initial state vector $\boldsymbol{\theta}_0$ is 8-dimentional random vector with mean $E[\boldsymbol{\theta}_0] = \bar{\boldsymbol{\theta}}_0$ and covariance $E\left[\left(\boldsymbol{\theta}_0 - \bar{\boldsymbol{\theta}}_0\right)\left(\boldsymbol{\theta}_0 - \bar{\boldsymbol{\theta}}_0\right)^T\right] = P_p^0$, measurement noise is zero-mean white Gaussion noises, $\mathbf{r}_{mp}^k \sim N\left[0, R_{mp}\right]$.

3.2 Nonlinear RC respiratory model

Fig. 1b shows the nonlinear RC respiratory model with non-invasive ventilatory pressure effect, $P_{ven}(t)$ and muscular pressure effect, $P_{mus}(t)$. In the model R represents the upper airway resistance as the biggest contribution to the resistive pressure lost comes from the upper airways. Rohrer's equation is used to compose the relation between airway flow $\dot{V}(t)$ and mouth pressure $P_{aw}(t)$. Thus resistive pressure lost and dynamic pressure across the nonlinear compliance C in the model can be given respectively as:

$$P_r(t) = \left(A_u + K_u\left|\dot{V}(t)\right|\right)\dot{V}(t) \tag{17}$$

$$P_c(t) = A_l e^{K_l V(t)} + B_l \tag{18}$$

where $V(t)$ represents the gas volume changes above Residual Volume in the lungs. In (7) and (8) A_u, K_u, A_l, K_l, B_l together with $P_{mus\,\mathbf{max}}$ constitute the unknown parameter vector to be estimated.

In the nonlinear RC model, parameter vector and state vector can be defined respectively as: $\boldsymbol{\theta}_k = \left[A_u \quad K_u \quad A_l \quad K_l \quad B_l \quad P_{mus\,\mathbf{max}}\right]^T$, $\mathbf{x}_s^k = \left[V^k\right]^T$. If the circuit theory rules are applied to the nonlinear RC circuits and elemental equations are written for nonlinear R and C elements below state-observation equations in discrete-time are given for the states of the circuits:

$$\mathbf{x}_s^{k+1} = V^k + \dot{V}^k + \mathbf{q}_{ns}^k \tag{19}$$

$$\mathbf{z}^k = \left(A_u + K_u\left|\dot{V}^k\right|\right)\dot{V}^k + A_l e^{K_l V^k} + B_l + P_{ven}^k - P_{mus}^k + \mathbf{r}_{ns}^k \tag{20}$$

where same assumptions on the state are applied to (19) and (20). Measurement noise and state noise are zero-mean white Gaussion noises, $\mathbf{q}_{ns}^k \sim N[0, Q_{ns}]$ and $\mathbf{r}_{ns}^k \sim N[0, R_{ns}]$. $\mathbf{z}^k$ is the measured mouth pressure sequence (discrete form of $P_{aw}(t)$).

Parameter model state equation of the nonlinear RC model is the same as the linear Mead model parameter equation (15) due to the same assumptions whereas (20) is used for the parameter model observation equation.

4. Dual UKF based respiratory model parameter estimation

Respiratory models, illustrated in Fig. 1 are composed of the electrical elements that have the unknown parameters. Discrete-time equations (13) – (16) were driven from Mead respiratory model and equations (15), (19) and (20) constitute non-linear RC respiratory model state-observation equations. The common way to model the respiratory system is to estimate the model parameters. The states are also required in order to implement Bayesian data analysis. Then, the respiratory model parameter estimation problem becomes dual recursive nonlinear inference problem from the noisy observed time series.

4.1 Data acquisition and pre-processing

In Mead model two state-observation equations for the states and parameters required to use dual UKF evaluation whereas joint UKF method was used for the nonlinear RC model. Both model parameters and states were estimated by *i)* artificially produced data that mimic the respiratory diseased patients, *ii)* data acquired from COPD patients and *iii)* data recorded from healthy subjects. Artificial airway flow was simulated as a sinusoidal signal with maximum flow of $0.6\,l/s$ and sampling rate was $100\,Hz$. Inspiration time T_I was taken as $1\,s$ while total breath cycle was $3\,s$. The states and observations were computed by (13), (14), (19), (20) and the parameters shown in the Table 1. After the observation sequence was obtained the zero-mean white Gaussian observation noises with $R_{ms} = 0.02\,I_{5\times5}$ and $R_{ns} = 0.02$ were added to the Mead model and nonlinear RC model respectively.

Simulation	Parameter	Value	Model	Parameter	Value
Non-invasive Ventilator Pressure Simulation	$PEEP$	$4\ cmH_2O$	Mead Model Parameters $\boldsymbol{\theta}$	R_c	$1.9601\ cmH_2O \cdot s \cdot l^{-1}$
	P_{ps}	$6\ cmH_2O$		L	$20.772\ cmH_2O \cdot s^2 \cdot l^{-1}$
	τ_{vi}	$0.006\ s$		C_l	$4.5182\ l \cdot cmH_2O^{-1}$
	τ_{ve}	$0.006\ s$		C_b	$6.6670\ l \cdot cmH_2O^{-1}$
	t_{trig}	$N/10$		R_p	$4.7039\ cmH_2O \cdot s \cdot l^{-1}$
	N_I	$N/3$		C_w	$7.56\ l \cdot cmH_2O^{-1}$
	N	300 points		C_e	$40.589\ l \cdot cmH_2O^{-1}$
Muscular Pressure Simulation	$P_{mus\,\max}$	$1.2\ cmH_2O$	Nonlinear RC Model Parameters $\boldsymbol{\theta}$	A_u	$3.1\ cmH_2O \cdot s \cdot l^{-1}$
	τ_m	$60\ ms$		K_u	$0.32\ cmH_2O \cdot s^2 \cdot l^{-2}$
Common Parameters	f_s	100 Hz		A_l	$0.5\ cmH_2O$
	$\mathbf{R}_s$	$0.02\ I$		K_l	0.2
	$\mathbf{Q}_s$	$0.01\ I$		B_l	$0\ cmH_2O$

Table 1. Parameters of the artificial respiratory signal.

Seven male and one female patients with COPD and four male and two female healthy non-smoking subjects (without any respiratory disease) were recruited. Patients were on non-invasive ventilator (Respironics Inc. BIPAP S/T IPAP - $8-15\,cmH_20$, PEEP - $0-4\,cmH_20$)

via facemask (Respironics Inc. Spectrum size medium and small). Mask pressure and airway flow were measured by pneumotachograph and pressure transducer system (Hans Rudolph Inc. Research pneumotachograph system). Sampling rate was 100 *Hz*. During acquisition, subjects were awake and in supine position breathing though the facemask. At least 10 breathing cycle of airway flow mask pressure and lung volume (integration of airflow) signals were recorded by data acquisition system (National Instrument DAQCard-6036E ADC-16bit) to the computer for the offline signal processing.

The airflow signal was first software filtered to remove high frequency noise with 8th order Butterworth low-pass filter with cut-off frequency of 50 *Hz* and then processed to detect the breathing cycle onset and end. Recorded signals were divided by breathing cycles with the consideration of ventilator trigger time, inspiration time and expiration time. Five clear breathing cycles were chosen for the offline signal processing step.

Dual UKF and joint UKF algorithm are applied to the pre-processed respiratory signals as explained in the section (3.2) and (3.3). Parameter constraints information was also incorporated in the dual UKF and EKF algorithm.

4.2 UKF and EKF parameter selection

Although there is no defined criteria for the estimator parameter selection, incorporating the model knowledge with the observation method some information can be drawn. In the both model the state transitions were obtained from the discretization of the continuous-time model equations by first-order Taylor series. The truncation error ($O(\Delta t^2)$) is the most contribution error in the process equation. Thus based on $\Delta t = 1/100\ s$, process noise covariance matrices for the states were $\mathbf{Q}_{ms} = 10^{-4}\, I_{5\times 5}$ and $\mathbf{Q}_{ns} = \begin{bmatrix} \mathbf{10^{-4}} & 0 \\ 0 & \mathbf{0} \end{bmatrix}$. In the UKF algorithm initial error covariance matrices for both models were $\mathbf{P}_0^{ms} = \mathbf{Q}_{ms}$ and $\mathbf{P}_0^{ns} = \mathbf{Q}_{ns}$ whereas in EKF in order to have some convergences in the parameters, initial error covariance were set to higher values such as $\mathbf{P}_0^{ms} = 10^6 \mathbf{Q}_{ms}$, and $\mathbf{P}_0^{ns} = 10^2 \mathbf{Q}_{ns}$. Observation noise covariance matrices were set with the convergence considerations to $\mathbf{R}_{ms} = \mathbf{R}_{ns} = 0.9$ for both models and for both estimators. Since the errors driven from the measurement equipment treats relatively low variances (accuracy of the equipments are in the range of %3), such a high choice of observation noise demonstrated the bigger uncertainty in the model fit to the measured noisy time-series. On the other hand in Mead model, the parameter observation error covariance matrix was set to the state process error covariance matrix due to the same equations.

Parameter and state initial values were found to be the most important settings. Especially the success of EKF was very much depended on the initial values. For the Mead model the initials were selected with regard to the convergences. Thus the set of initials for the Mead model were drawn from $\mathbf{x}_0^s = \mathbf{0}$, $\mathbf{x}_0^p \sim N[1,1]$ for UKF algorithm and $\mathbf{x}_0^s = \mathbf{0}$, $\mathbf{x}_0^p \sim N[1,2]$ for EKF algorithm. For the nonlinear RC model initials were the same for the states, but for the parameters, the $\mathbf{x}_0^p \sim N[0,1]$ was set in the both estimator algorithms.

Furthermore, UKF algorithm parameters were set according to the minimum Mean Squared Error (MSE) computed in the artificial data run. Monte Carlo simulations were performed with 100 run by artificial data series. $\alpha = 0.1$ for the parameters whereas $\alpha = 0.9$ for the states. κ, the secondary adjustment parameter was set to 1.1 for the minimum MSE. Finally, $\beta = 2$ indicating that the actual acquired signals were Gaussian distributed.

5. Results

5.1 MSE for the Mead and nonlinear RC models

MSE is the important showing for the performance comparison of both estimators. It was calculated with the Monte Carlo simulations and plotted against the data points. Figs. 2 and 3 show the MSE curves for the Mead and nonlinear RC models respectively. Both UKF and EKF estimates converge to single points through time-steps. Compared to Figs 2 and 3, although Mead model convergences are faster than nonlinear RC model convergences, approximations are better in the nonlinear RC model meaning that corresponding MSEs are lower. However, parameters K_u , K_l in the nonlinear RC model and $P_{mus\,\max}$ in the Mead model show very irregular results that demonstrate very slow or no convergence at all. This can be explained by the parameters interaction in the model structure. Parameter K_u is effected by the uncertainty of the airway flow, $\dot{V}^k$ by nonlinear fashion and K_l is in the direct relation with the estimated state V^k. On the other hand, parameter L is found to be the less identifiable parameter, apart from C_e. Since the state transition model of $P_{mus\,\max}$ includes L in the Mead model, $P_{mus\,\max}$ uncertainty is mostly effected by this parameter, therefore, degeneracy of the convergence happened.

It is apparent from the Figures that UKF converge faster than EKF for the Mead model. However, for the nonlinear model, EKF showed surprisingly no convergence at all for the nonlinear parameters A_l , K_l and B_l. This could be the consequence of the changes in the expiration. As it is noted convergences are distorted when the expiration begins and at the

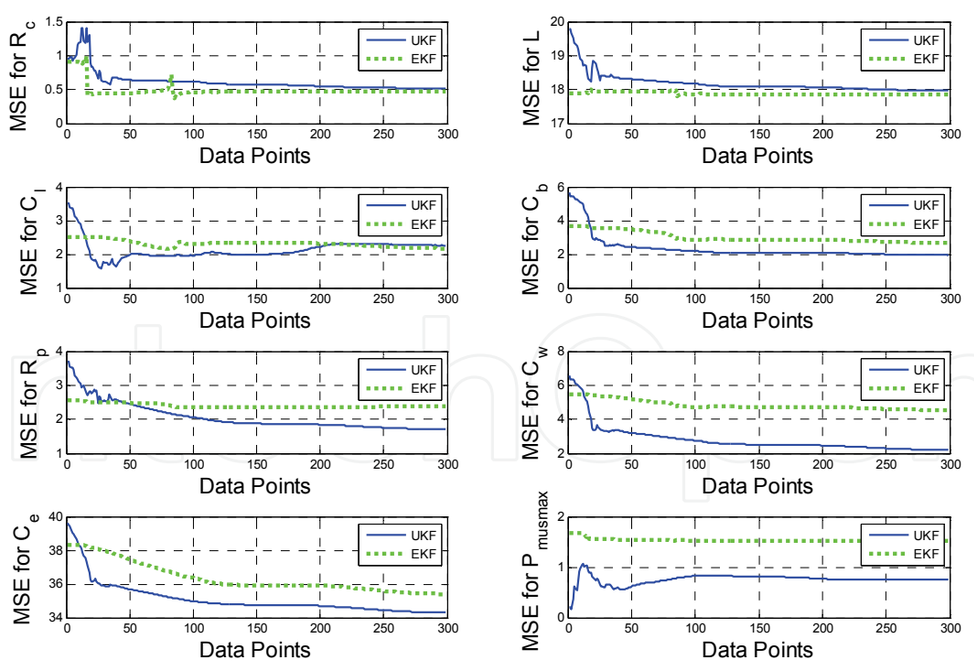

Fig. 2. MSE curves belongs to Mead model parameters (produced by artificial data). Curves were calculated by 100 run Monte Carlo simulations. Continuous and dashed lines represent the UKF and EKF estimates respectively.

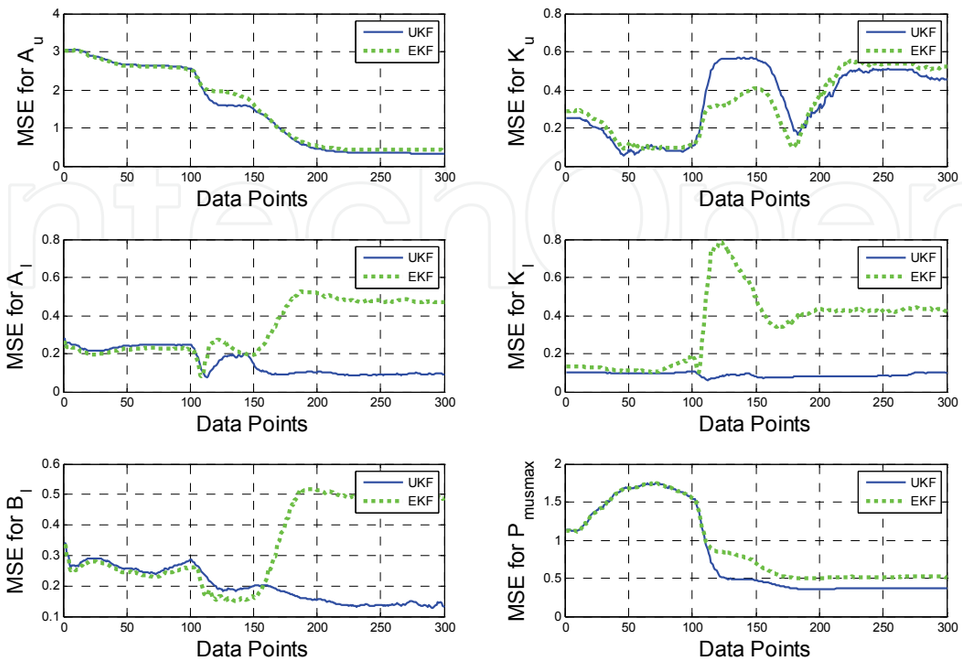

Fig. 3. MSE curves belongs to nonlinear RC model parameters (produced by artificial data). Curves were calculated by 100 run Monte Carlo simulations. Continuous and dashed lines represent the UKF and EKF estimates respectively.

expiration side only the nonlinear parameters govern the equations leaving muscular and ventilatory effects without contribution. Also, in line with our previous study (Saatci & Akan, 2007) in the nonlinear RC model, the most robust parameter is the parameter $P_{mus\,\max}$ for the artificial data sequence.

5.2 Convergence of the parameters for the measured respiratory signals

To illustrate the performance of the UKF and EKF estimators for the case of measured signals, parameters were estimated from acquired respiratory signals. Both UKF and EKF were evaluated with both model and for COPD patients' data and for healthy subjects' data. Figs 4 and 5 show Mead model UKF and EKF parameter convergence curves produced by the representative COPD patient's data respectively. Estimations from five different breath cycles were plotted on the same figure to illustrate the similarities and differences between breath cycles. Figs 6 and 7 show the plots of the same patients' parameters for the nonlinear RC model. Parameters' convergence curves produced by the healthy subject's data were plotted in the Figs 8 and 9 corresponding to the Mead model and in the Figs 10 and 11 for the nonlinear RC model.

First, it should be noted that since the Figs 4, 5, 6, 7 belong to the same COPD patient's data and it is expected to see compatible parameter values that at least indicate the patient's

actual respiratory condition. First, if we compare Fig. 4 and Fig. 5 for some parameters EKF doesn't seem to converge at all in the Mead model. Since the initial value is very important for the EKF to converge, initial error covariance matrix was set to high values ($\mathbf{P}_0^{mp} = 10^1$ and $\mathbf{P}_0^{np} = 10^1$) in order to compensate the initial uncertainty. Thus, although consistency between breath cycles is accomplished in the EKF, the actual convergences don't go very far from the initial values. However for the nonlinear RC model case (Figs. 6 and 7), the parameter estimates of EKF and UKF is not only consistent but also very selective. Breath-to-breath variations existed for $P_{mus\,\max}$ could be the consequence of the variations in the patient's breath cycle.

If healthy subject's data is examined, it could be seen that convergence problems of the EKF resulted in again unexpected values in the Mead model (Figs 8 and 9). However, subject's data sequence fit to nonlinear RC model successfully. From the estimated values of the parameters it is apparent that UKF and EKF perform identical for the nonlinear RC model in both COPD patient's data and healthy subject's data.

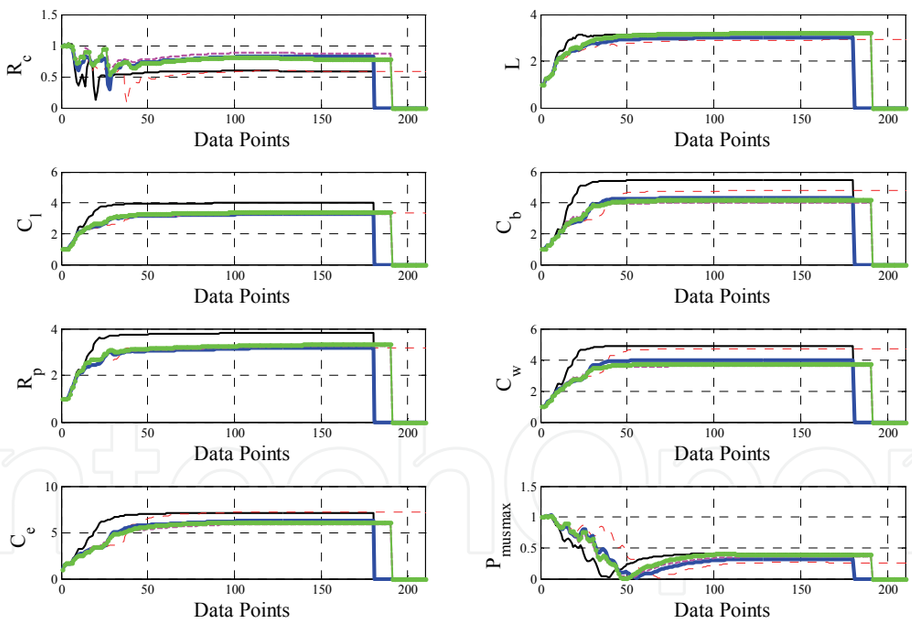

Fig. 4. Mead model UKF parameter convergence curves (produced by the representative COPD patient's data). Estimations from five different breath cycles were plotted on the same figure to illustrate the similarities and differences between breath cycles

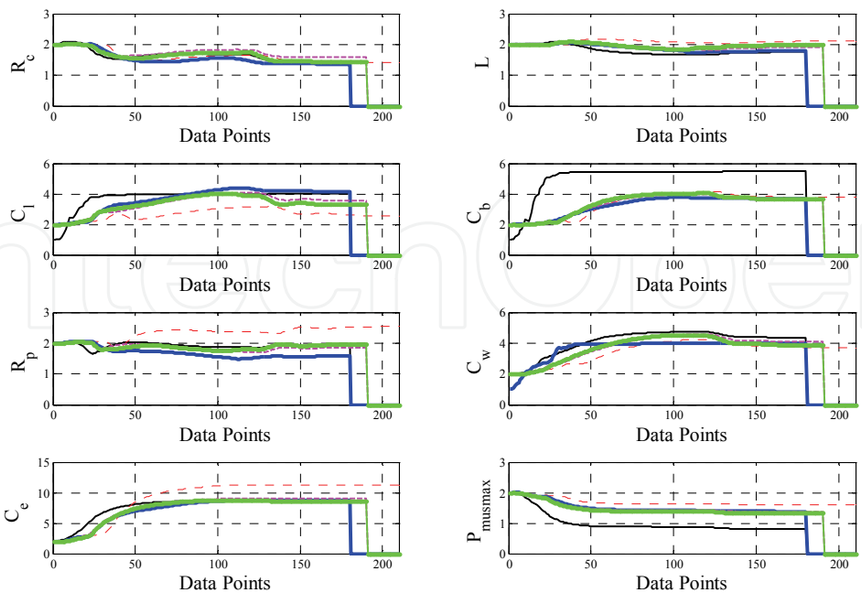

Fig. 5. Mead model EKF parameter convergence curves (produced by the representative COPD patient's data). Estimations from five different breath cycles were plotted on the same figure to illustrate the similarities and differences between breath cycles

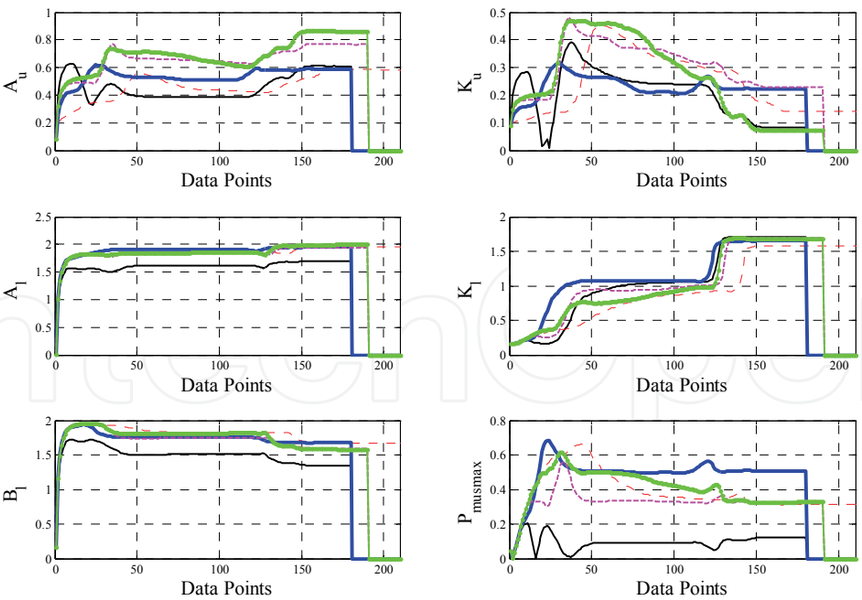

Fig. 6. Nonlinear RC model UKF parameter convergence curves (produced by the representative COPD patient's data). Estimations from five different breath cycles were plotted on the same figure to illustrate the similarities and differences between breath cycles

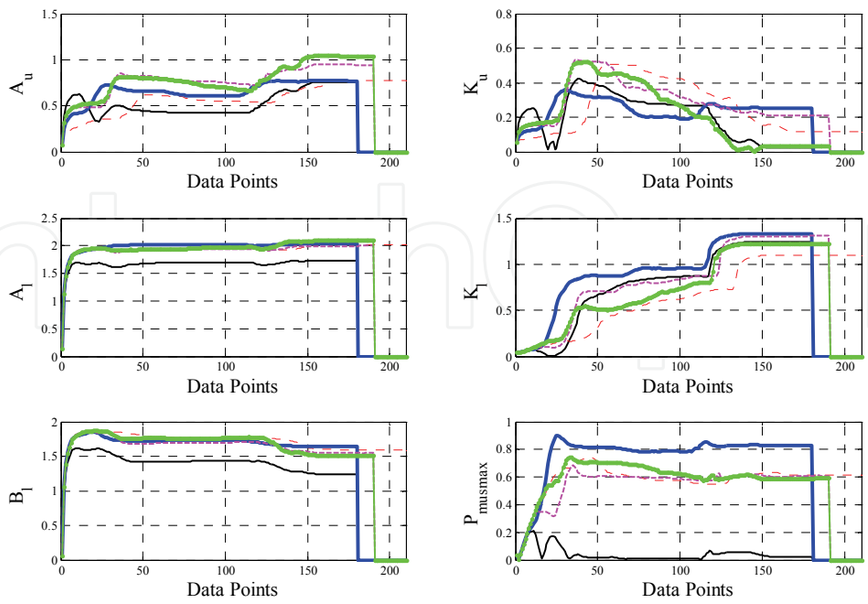

Fig. 7. Nonlinear RC model EKF parameter convergence curves (produced by the representative COPD patient's data). Estimations from five different breath cycles were plotted on the same figure to illustrate the similarities and differences between breath cycles

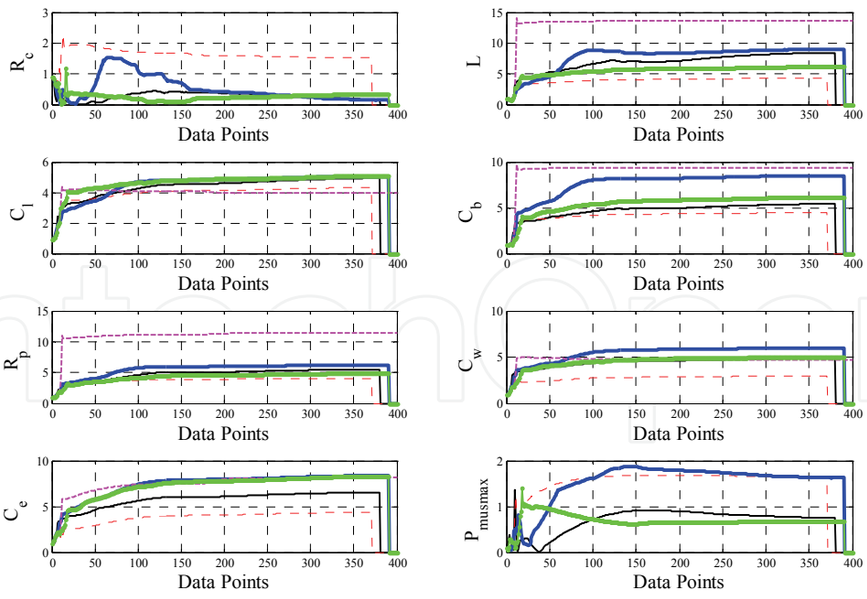

Fig. 8. Mead model UKF parameter convergence curves (produced by the representative healthy subject's data). Estimations from five different breath cycles were plotted on the same figure to illustrate the similarities and differences between breath cycles

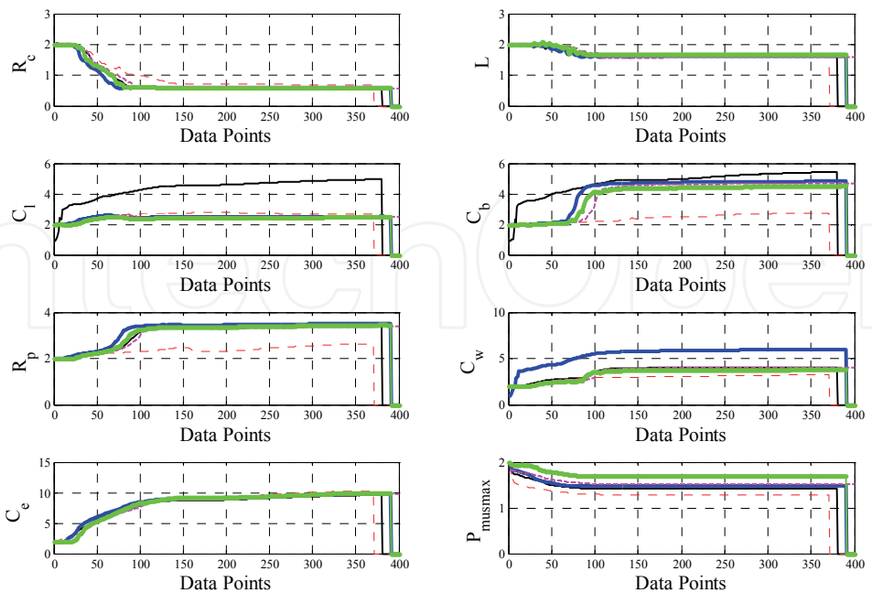

Fig. 9. Mead model EKF parameter convergence curves (produced by the representative healthy subject's data). Estimations from five different breath cycles were plotted on the same figure to illustrate the similarities and differences between breath cycles

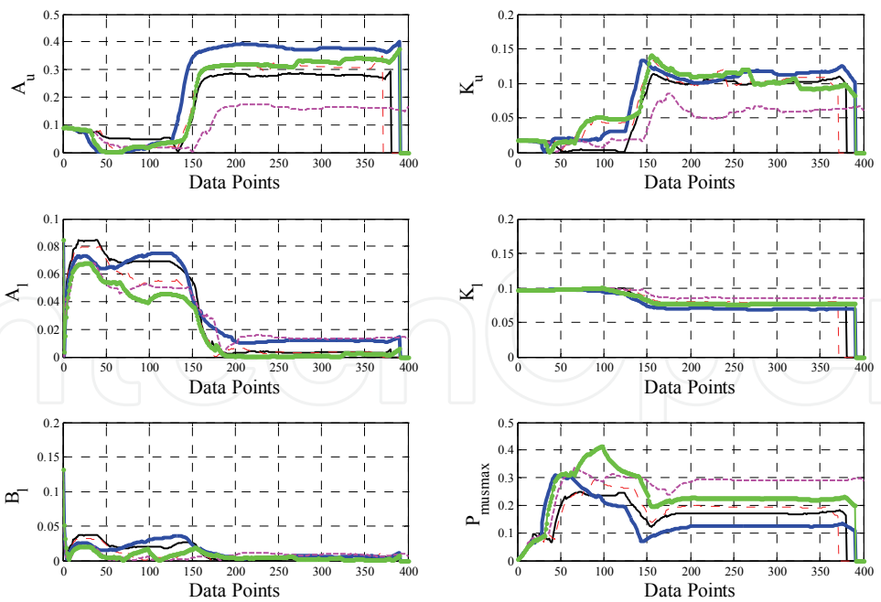

Fig. 10. Nonlinear RC model UKF parameter convergence curves (produced by the representative healthy subject's data). Estimations from five different breath cycles were plotted on the same figure to illustrate the similarities and differences between breath cycles

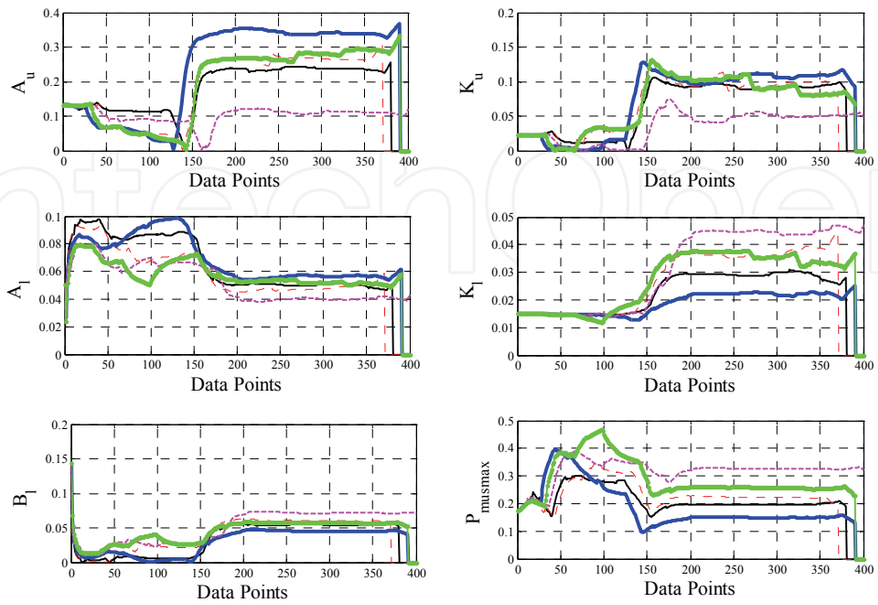

Fig. 11. Nonlinear RC model EKF parameter convergence curves (produced by the representative healthy subject's data). Estimations from five different breath cycles were plotted on the same figure to illustrate the similarities and differences between breath cycles

5.3 Convergence of the states for the measured respiratory signals

Reproducibility of the defined states of the respiratory models was also verified by comparing the state estimates produced for five breath cycles. Figures 12 and 13 show the Mead model states of the COPD patient corresponding to UKF and EKF estimates respectively. Healthy subject's figures are given in the Figs 14 and 15. Comparing to both figures, contrary to parameter estimates EKF seems to be more successful than UKF in the time-varying state estimation. For instance, state $\dot{V}_L^k$ could be estimated nothing but noise by UKF in the Mead model. Moreover, tracking of the states $P_{C_l}^k$, $P_{C_b}^k$ and $P_{C_w}^k$ converged to unexpectively more negative pressure values by UKF. However, incorporating the model equations together with the lung tissue, small airways and chest wall pressure effects it is expected to see pressure rise at the inspiration and pressure decrease at the expiration. Thus, especially EKF tracks produced from healthy subject's data (Fig. 15) report the expected state pressure waveforms in the Mead model.

In the nonlinear RC model case, both estimation methods again demonstrate the same sate tracks. Figs 16 and 17 are the evident of the UKF and EKF success on the state estimation. Tracks show expected lung volume, above Residual Volume, V_L^k as it increases through inspiration and decreases to zero at the end of expiration.

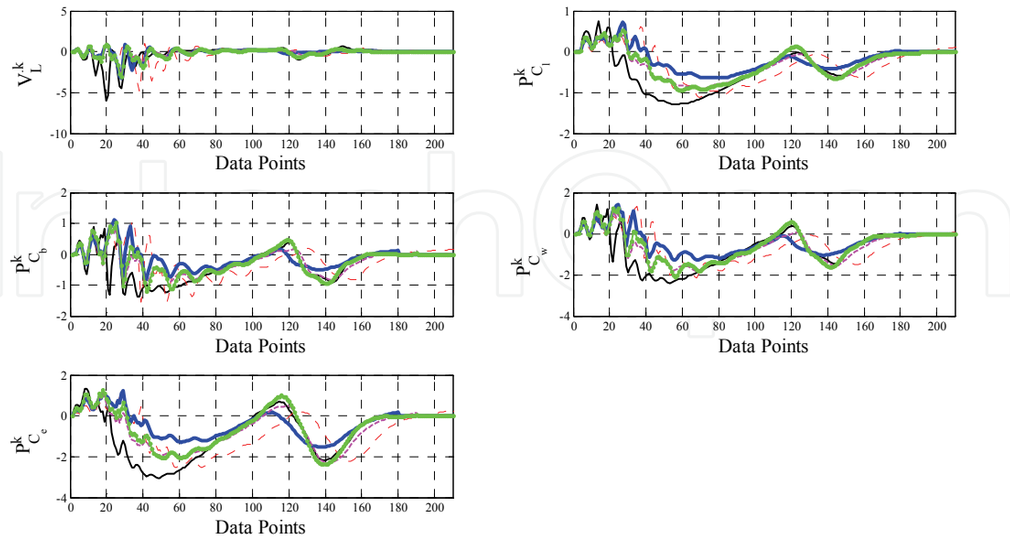

Fig. 12. Mead model UKF state convergence curves (produced by the representative COPD patient's data). Estimations from five different breath cycles were plotted on the same figure to illustrate the similarities and differences between breath cycles

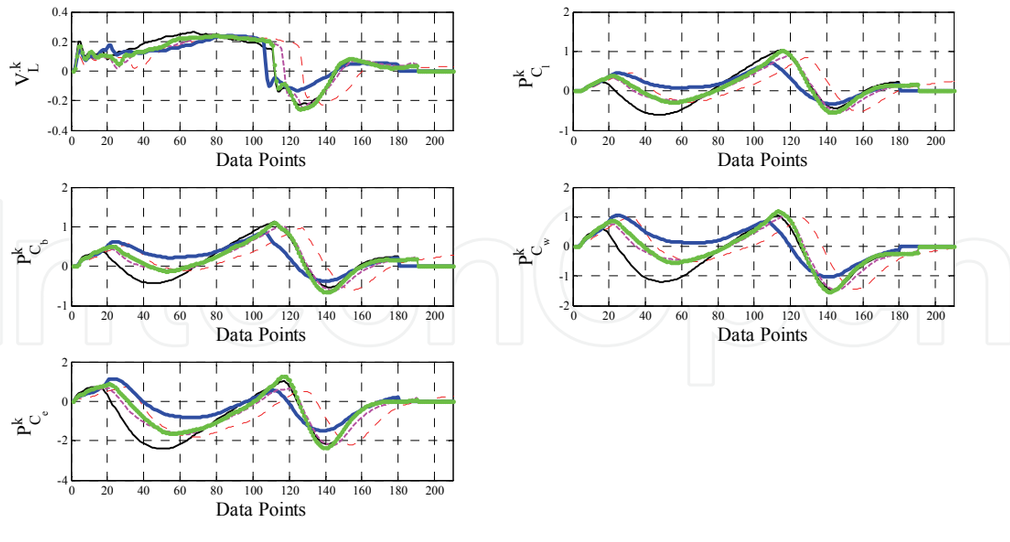

Fig. 13. Mead model EKF state convergence curves (produced by the representative COPD patient's data). Estimations from five different breath cycles were plotted on the same figure to illustrate the similarities and differences between breath cycles

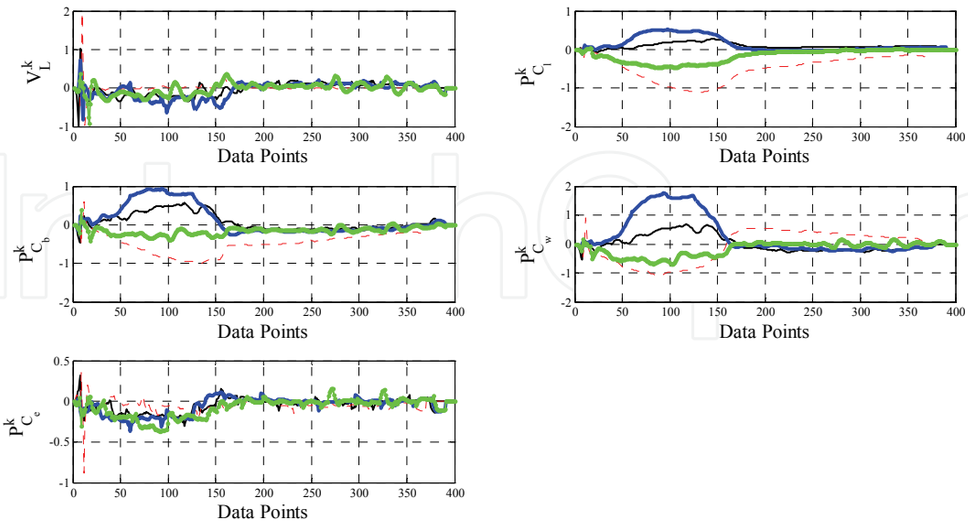

Fig. 14. Mead model UKF state convergence curves (produced by the representative healthy subject's data). Estimations from five different breath cycles were plotted on the same figure to illustrate the similarities and differences between breath cycles

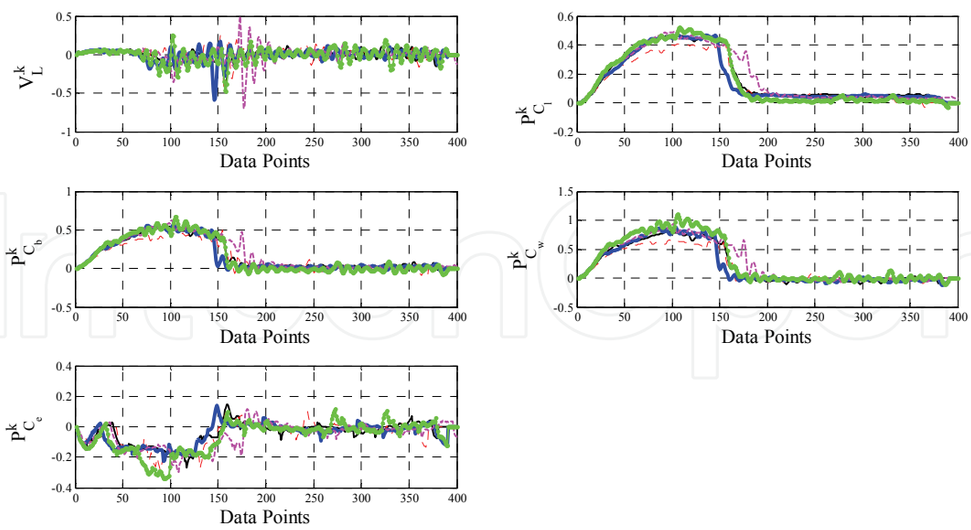

Fig. 15. Mead model EKF state convergence curves (produced by the representative healthy subject's data). Estimations from five different breath cycles were plotted on the same figure to illustrate the similarities and differences between breath cycles

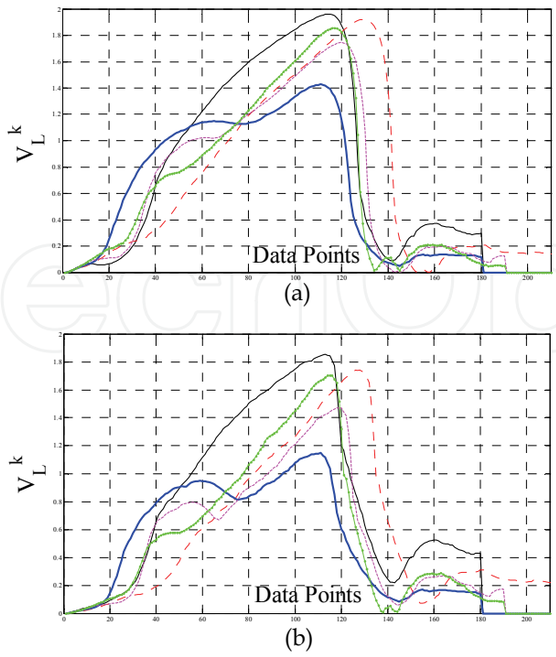

Fig. 16. Nonlinear RC model (a) UKF and (b) EKF parameter convergence curves (produced by the representative COPD patient's data). Estimations from five different breath cycles were plotted on the same figure.

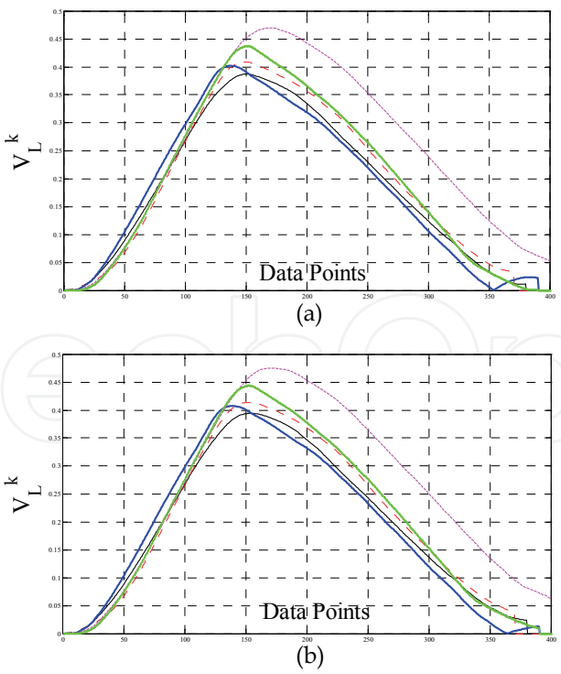

Fig. 17. Nonlinear RC model (a) UKF and (b) EKF parameter convergence curves (produced by the representative healthy subject's data). Estimations from five different breath cycles were plotted on the same figure.

6. Conclusion

Common problem in the respiratory model parameter estimates is the lack of information on the uncertainty (or residuals) between measured airway pressure and used model. As the model has more degree of freedom (incorporates more parameter (Avanzolini et al., 1995) or incorporates the nonlinearity (Athanasiades et al., 2000)) the uncertainties approaches to the statistical noise that is usually Gaussian distributed. Here, we started with the assumption that the residuals are the white Gaussian noises and estimation and measured noisy time series can be fit to the respiratory models by the estimation methods. Thus, unscented Kalman filter (UKF) was employed as an inverse solver to estimate the time-invariant parameters and time-varying states in the linear Mead model and the nonlinear RC model. Illustrative comparison between UKF and conventional EKF was also performed with the respiratory model applications. The convergence results of the parameters demonstrated the performance gains over EKF only in the Mead model. UKF is known to make more accurate results only if the kurtosis and higher order moments of the parameters' errors are significant. This fact is one indication of why the UKF doesn't perform better than EKF in the nonlinear RC model parameter and state estimation.

It is also experienced that the tuning of EKF is more difficult than UKF even though UKF has more tuning parameter. For the real respiratory signals, initial parameter and state vectors may require small adjustments for the proper convergences of the parameters.

7. References

Athanasiades, A.; Ghorbel, F. & Clark, J.W. (2000). Energy analysis of a nonlinear model of the normal human lung. *Journal of Biological Systems*, Vol.8, 115-139, ISSN 02183390

Arulampalam, M.S.; Maskell, S.; Gordon, N. & Clapp, T. (2002). A tutorial on particle filters for online nonlinear/non-Gaussian Bayesian tracking. *IEEE Transactions on Signal Processing*, Vol.50, No.2, February 174-188, ISSN 10535888

Avanzolini, G.; Barbini, P.; Cappello, A. & Cevenini, G. (1995). Influence of flow pattern on the parameter estimates of a simple breathing mechanics model. *IEEE Transactions on Biomedical Engineering*, Vol.42, No.4, April 394-402, ISSN 00189284

Avendano, L.E.; Castellanos, C.G. & Ferrero, J.M. (2006). Spectrum estimation and adaptive denoising of electrocardiographic signals using Kalman filters. *Computers in Cardiology*, Vol.33, 925-928, ISSN 02766547

Bates, J.H.Y. & Lutchen K.R. (2005). The interface between measurement and modelling of peripheral lung mechanics. *Respiratory Physiology & Neurobiology*, Vol.148, 153-164,

Brochwell, A.E., Kass, R.E. & Schwartz, A.B. (2007). Statistical signal processing and the motor cortex. *Proceedings of the IEEE*, Vol.95, No.5, May 881-898, ISSN 00189219

Chen, Z. (2003). Bayesian filtering: from Kalman filters to particle filters, and beyond. tech. rep. Adaptive Syst. Lab., McMaster University, Hamilton, ON, Canada

Chow, S.; Ferrer, E. & Nesselroade, J.R. (2007). An unscented Kalman filter approach to the estimation of nonlinear dynamical systems models. *Multivariate Behavioral Research*, Vol.42, Issue.2, June 283-321, ISSN 15327906

Diong, B., Nazeran, H., Nava, P. & Goldman M. (2007). Modeling human respiratory impedance. *IEEE Engineering in Medicine and Biology Magazine*, Vol.26, January 48-55, ISSN 07395175

Grewal, M.S. & Andrews, A.P. (2001). *Kalman Filtering: Theory and Practice*, Wiley, ISBN 0471392545, USA

Hellinckx, J.; Cauberghs, M. & De Boeck, K. (2001). Evaluation of impulse oscillation system: comparison with forced oscillation technique and body plethysmography. *European Respiratory Journal*, Vol.18, 564-570

Ijaz, U.Z.; Khambampati, A.K.; Lee, J.S.; Kim, S. & Kim, K.Y. (2008). Nonstationary phase boundary estimation in electrical impedance tomography using unscented Kalman filter. *Journal of Computational Physics*, Vol.227, 7089-7112, ISSN 00219991

Julier, S.J. & Uhlmann, J.K. (1997). A new extension of the Kalman filter to nonlinear systems. *Proceedings of Int. Symp. Aerospace/Defence Sensing, Simul. and Controls*, Orlando, FL

Kandepu, R.; Foss, B. & Imsland, L. (2008). Applying the unscented Kalman filter for nonlinear state estimation. *Journal of Process Control*, Vol.18, 753-768, ISSN 09591524

Lutchen, K.R. & Costa, K.D. (1990). Physiological interpretations based on lumped element models fit to respiratory impedance data: use of forward-inverse modelling. *IEEE Transactions on Biomedical Engineering*, Vol.37, No.11, November 1076-1086, ISSN 00189294

Moradkhani, H.; Sorooshian, S.; Gupta, H.V. & Houser, P.R. (2005). Dual state-parameter estimation of hydrological models using ensemble Kalman filter. *Advances in Water Resources*, Vol.28, 135-147, ISSN 03091708

Nucci, G.; Tessarin, S. & Cobelli, C. (2002). A morphometric model of lung mechanics for time-domain analysis of alveolar pressures during mechanical ventilation. *Annals of Biomedical Engineering*, Vol.30, 537-545, ISSN 00906964

Polak, A.G. & Mroczka J. (2006). Nonlinear model for mechanical ventilation of human lungs. *Computers in Biology and Medicine*, Vol.36, 41-58, ISSN 00104825

Saatci, E. & Akan, A. (2007). Lung model parameter estimation by unscented Kalman filter. *Proceedings of the 29th Annual International Conference of the IEEE EMBS*, Lyon, France, August 2556-2559

Sameni, R.; Shamsollahi, M.B.; Jutten, C. & Clifford G.D. (2007). A nonlinear Bayesian filtering framework for ECG denoising. *IEEE Transactions on Biomedical Engineering*, Vol.54, No.12, December 2172-1285, ISSN 00189294

Vauhkonen, M.; Karjalainen, P.A. & Kaipio, J.P. (1998). A Kalman filter approach to track fast impedance changes in electrical impedance tomography. *IEEE Transactions on Biomedical Engineering*, Vol.45, No.4, April 486-493, ISSN 00189294

Wan, E.A. & Merwe, van der R. (2001). The unscented Kalman filter, In: *Kalman Filtering and Neural Networks*, Simon Haykin, (Ed.), 221-283, Wiley, ISBN 0471369981, NewYork

Xiong, K.; Zhang, H.Y. & Chan, C.W. (2006). Performance evaluation of UKF- based nonlinear filtering. *Automatica*, Vol.42, 261-270, ISSN 00051098

Yamada, Y. & Du, H.L. (2000). Analysis of the mechanisms of expiratory asynchrony in pressure support ventilation: a mathematical approach. *Journal of Applied Physiology*, Vol.88, 2143-2150, ISSN 87507587

Yuan, H.; Suki, B. & Lutchen, K.R. (1998). Sensitivity analysis for evaluating nonlinear models of lung mechanics. *Annals of Biomedical Engineering*, Vol.26, 230-241, ISSN 00906964

Kalman Filter Recent Advances and Applications

Edited by Victor M. Moreno and Alberto Pigazo

ISBN 978-953-307-000-1
Hard cover, 584 pages
Publisher InTech
Published online 01, April, 2009
Published in print edition April, 2009

The aim of this book is to provide an overview of recent developments in Kalman filter theory and their applications in engineering and scientific fields. The book is divided into 24 chapters and organized in five blocks corresponding to recent advances in Kalman filtering theory, applications in medical and biological sciences, tracking and positioning systems, electrical engineering and, finally, industrial processes and communication networks.

InTech Europe
University Campus STeP Ri
Slavka Krautzeka 83/A
51000 Rijeka, Croatia
Phone: +385 (51) 770 447
Fax: +385 (51) 686 166
www.intechopen.com

InTech China
Unit 405, Office Block, Hotel Equatorial Shanghai
No.65, Yan An Road (West), Shanghai, 200040, China
中国上海市延安西路65号上海国际贵都大饭店办公楼405单元
Phone: +86-21-62489820
Fax: +86-21-62489821

IntechOpen